ROYAL SOCIETY
OF CHEMISTRY

PAPER

Check for updates

The influence of molecular conformation on the photophysics of organic room temperature phosphorescent luminophores†

Rongjuan Huang,[a] Jonathan S. Ward,[b] Nadzeya A. Kukhta,[b] João Avó,[c] Jamie Gibson,[d] Thomas Penfold,*[d] João C. Lima, [ID][e] Andrei S. Batsanov, [ID][b] Mário N. Berberan-Santos, [ID][c] Martin R. Bryce [ID][b] and Fernando B. Dias [ID] *[a]

A series of novel donor–acceptor–donor (D–A–D) compounds featuring dibenzothiophene (**DBT**) and phenothiazine (**PTZ**) units are presented. A different degree of steric hindrance between the donor and acceptor fragments is achieved by the systematic changes of donor substituents (methyl, iso-propyl, *tert*-butyl groups). This leads to the tuning of photophysical properties by conformational control. The unsubstituted **DPTZ–DBT** molecule exists in both equatorial and axial forms in the ground state, due to the ability of **PTZ** to form H-extra and H-intra folded conformers that allow formation of parallel quasi-axial (ax) and perpendicular quasi-equatorial (eq) conformers, respectively. However, the equatorial conformer prevails in the excited state. This leads to strong room temperature phosphorescence (RTP) in the green region with high phosphorescence quantum yield (60 ± 8%). Under the influence of bulky substituents, the alkyl-**DPTZ–DBT** derivatives change molecular conformation, preventing formation of the excited charge transfer state. Hence, blue, but much weaker, phosphorescence is observed. The less bulky methyl substituent on the donor results in dual RTP (blue and green), apparently violating Kasha's rule imposed by the modulation of the barriers between excited states. The experimental results are supported by DFT calculations in the ground and excited state. Control of conformation with substituents is an effective strategy for tuning the excited state properties of D–A–D molecules for RTP emission.

Introduction

Room-temperature phosphorescent (RTP) emitters have attracted great attention in recent years due to their potential for opto-electronic and photonic applications, such as in organic light-emitting diodes (OLEDs),[1–4] luminescence labels,[5] imaging,[6] sensing[7,8] and optical thermometry.[9,10] The emission from the triplet excited state involves a quantum mechanically forbidden spin flip, which is uncompetitive with the non-radiative relaxation *via* thermal and collisional processes.[11] The triplet state is,

[a] *Physics Department, Durham University, South Road, Durham, DH1 3LE, UK. E-mail: f.m.b.dias@durham.ac.uk*

[b] *Chemistry Department, Durham University, South Road, Durham, DH1 3LE, UK*

[c] *CQFM-IN and IBB-Institute for Bioengineering and Biosciences, Instituto Superior Técnico, Universidade de Lisboa, 1049-001 Lisboa, Portugal*

[d] *Chemistry-School of Natural and Environmental Sciences, Newcastle University, Newcastle upon Tyne, NE1 7RU, UK. E-mail: tom.penfold@newcastle.ac.uk*

[e] *REQUIMTE, Departamento de Química, Faculdade de Ciências e Tecnologia, Universidade Nova de Lisboa, 2829-516 Caparica, Portugal*

† Electronic supplementary information (ESI) available. CCDC 1846156–1846161. For ESI and crystallographic data in CIF or other electronic format see DOI: 10.1039/c8tc02987c

therefore, highly sensitive to temperature and strongly affected by the presence of molecular oxygen. However, achieving efficient RTP is possible when the intersystem crossing (ISC) from the lowest excited singlet (S₁) to the triplet state (T₁) is enhanced, and the non-radiative relaxation from T₁ to the ground state due to molecular vibrations is suppressed.[3]

Efficient RTP is obtained in organic–metal complexes due to the presence of heavy metals or halogens.[12] In these compounds the spin–orbit coupling (SOC) is enhanced due to the effect of heavy-atoms promoting ISC by mixing the molecular orbital configurations of singlet and triplet states. However, halogen–carbon bonds are weak and prone to photolytic cleavage, which could lead to less stable emitters. Additionally, RTP has been reported in compounds that do not contain heavy-metals, by using additional strategies to reduce vibrational quenching of the triplet population.[13] This is typically achieved by using rigid hosts, molecular crystals and molecular aggregation.[14,15] However, molecular design strategies to enhance ISC and RTP in metal-free molecules are still limited and relatively inefficient compared to heavy metals. This reflects the lack of detailed understanding of how alterations of molecular conformation, nuclei vibrations and substituents may affect the radiative

9238 | *J. Mater. Chem. C*, 2018, **6**, 9238–9247

This journal is © The Royal Society of Chemistry 2018

rate and the non-radiative internal conversion (IC), and ISC rates, as well as the corresponding yields for these processes. This information is relevant not only for RTP molecules, but also for emitters showing thermally activated delayed fluorescence (TADF), which are now routinely used in OLEDs.[16,17] In the latter, controlling the ISC and reverse ISC (RISC) rates has direct impact on device efficiency and stability. Fast ISC/RISC rates are preferable to promote efficient triplet harvesting and obtain shorter-lived excited states.[18] This is key to suppressing the efficiency roll-off observed in OLEDs.[19,20] Detailed investigations of molecular structure–property relationships are thus needed to guide synthetic strategies for the design of more efficient RTP and TADF emitters.

Herein is reported the synthesis, computation and photophysics of four donor–acceptor–donor (D–A–D) metal-free, and halogen-free, organic molecules, which are based on phenothiazine (**PTZ**) and dibenzothiophene (**DBT**) moieties as the electron donor (D) and acceptor (A) units, respectively. These are the unsubstituted parent molecule, **DPTZ–DBT**, and the three analogues, **DPTZ–Me–DBT**, **DPTZ–ⁱPr–DBT**, and **DPTZ–ᵗBu–DBT**, substituted with methyl, iso-propyl and *tert*-butyl groups at the C1-position of each **PTZ** unit. These molecules show profoundly different excited state properties due to the different conformations (axial *vs.* equatorial)[21] imposed by the effect of steric hindrance around the D–A bonds. These equatorial and axial conformers have been identified recently in related compounds, showing different RTP and TADF responses.[22]

Results and discussion

Molecular design, synthesis and structures

Fig. 1 shows the molecular structures of the four D–A–D compounds studied in this work. These molecules were rationally designed based on the following considerations. (i) **PTZ** is a donor unit in many luminescent materials,[23–26] and emits phosphorescence at room temperature in solid zeonex films;

(ii) **DBT** is also a standard luminophore, although usually serving as an electron donor in combination with acceptor units, *e.g.* fluorene,[27,28] anthracene,[29] or benzoyl.[30] Its use as an acceptor in the present series of compounds is, therefore, unusual, although there is precedent with the bis((3,6-di-*t*-butyl)*N*-carbazolyl) derivative reported previously.[3,31] The **DBT** unit has been previously identified as promoting fast RISC;[3] (iii) these four molecules are direct analogues of the dibenzothiophene-*S,S*-dioxide series which possess an unusual combination of TADF and RTP.[32] The key distinction with the present series is the different oxidation state of the thiophene sulfur (S in the present work; SO₂ in the previous study).[32] The SO₂ unit imparts strong acceptor properties with a much lower LUMO and increased charge-transfer properties compared to the present dibenzothiophene series. The 2,8-disubstitution of **DBT** (**PTZ** *para* to the sulfur) was chosen to maximize the interaction of the D and A units, compared to the isomeric 3,7-derivatives (**PTZ** units *meta* to sulfur);[3,31,33] (iv) both **PTZ** and **DBT** units on their own have potential to show strong triplet formation properties, due to the presence of the sulfur and nitrogen atoms;[3,32] (v) the increasing steric hindrance imparted by the alkyl substituents on the **PTZ** units serves as a probe of steric effects on the conformation of the D–A–D system and its effect on the ISC/RISC rates as discussed in more detail below.

The syntheses of **DPTZ–DBT**, **DPTZ–Me–DBT**, **DPTZ–ⁱPr–DBT** and **DPTZ–ᵗBu–DBT** are presented in the ESI.† Their structures and high purity were unambiguously established by a combination of NMR spectroscopy, mass spectrometry, elemental analysis and single-crystal X-ray analysis (ESI†).

The X-ray molecular structures of **DPTZ–DBT**, **DPTZ–Me–DBT** and **DPTZ–ⁱPr–DBT** revealed interesting conformational properties of the molecules in the solid state. The structures of **DPTZ–DBT** and **DPTZ–ⁱPr–DBT** show that the **PTZ** units are exclusively in equatorial and axial conformations, respectively, see Fig. 2. This is in agreement with the calculations of the relative energies of each conformer for all 4 molecules shown in Table S1 (ESI†).
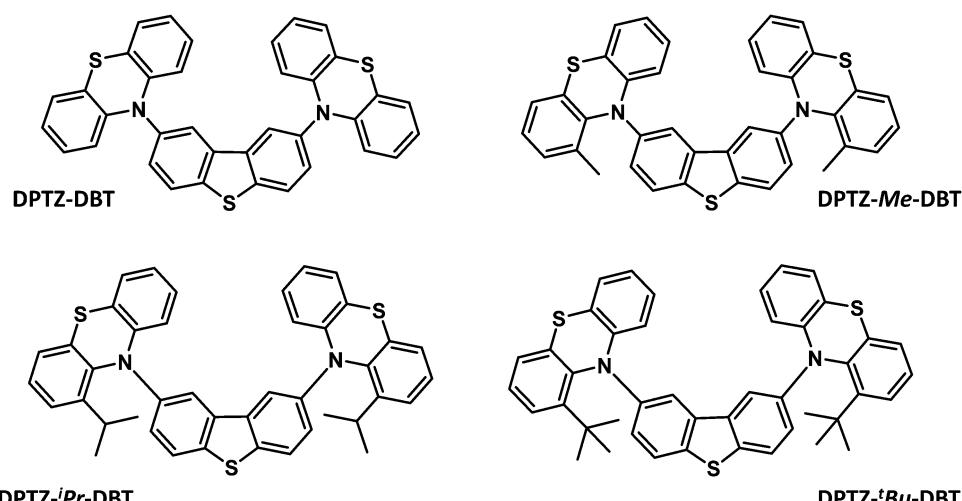
Fig. 1 Molecular structures of the compounds studied in this work.

This journal is © The Royal Society of Chemistry 2018

J. Mater. Chem. C, 2018, **6**, 9238–9247 | 9239
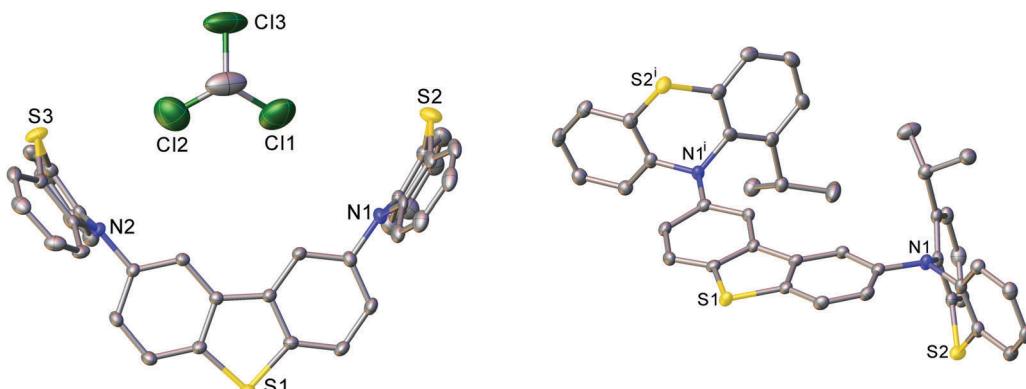
Fig. 2 X-ray molecular structures of **DPTZ–DBT**·CDCl₃ (left) and **DPTZ–ⁱPr–DBT** (right) showing equatorial and axial **PTZ** groups, respectively. Thermal ellipsoids are drawn at the 50% probability level; H atoms are omitted; primed atoms are generated by the twofold axis.

However, in the polymorphic structures of **DPTZ–Me–DBT** there is conformational disorder of the **PTZ** units. This is consistent with the dual phosphorescence observed in **DPTZ–Me–DBT** which is ascribed to the low energy barrier to subtle molecular vibrations (see discussion below). Additional figures, discussion and tables of dihedral angles in the X-ray structures are shown in Section S6 (ESI†).

Photophysics

In Fig. 3a the absorption and emission spectra of **DPTZ–DBT** and **DPTZ–ⁱPr–DBT** are compared in toluene solution. The absorption spectrum of **DPTZ–ⁱPr–DBT** shows three well-defined transitions. These consist of low energy bands around 380 nm and 320 nm, and a higher energy transition below 300 nm, which is not entirely observed in toluene, due to the solvent cut-off.

Similar bands are observed in the absorption spectra of the other substituted molecules, **DPTZ–Me–DBT** and **DPTZ–ᵗBu–DBT** (Fig. S2, ESI†). The onset of the absorption spectrum of the unsubstituted **DPTZ–DBT** is around 400 nm, with the absorption intensity growing smoothly, up to the point where the peak of the lower energy band at 320 nm is reached. A second absorption band is also observed below 300 nm, as in the substituted molecules. However, in clear contrast with the substituted molecules, no well-defined band peaking at 380 nm is observed in **DPTZ–DBT**. The two transitions at 320 nm and below 300 nm, also identified in the substituted compounds, are the signatures of the individual **PTZ** and **DBT** units, respectively, as shown in Fig. S2 (ESI†). The low energy band is observed only in the absorption spectra of the substituted molecules and not in the spectra of either **PTZ** or **DBT**. This low energy band is also
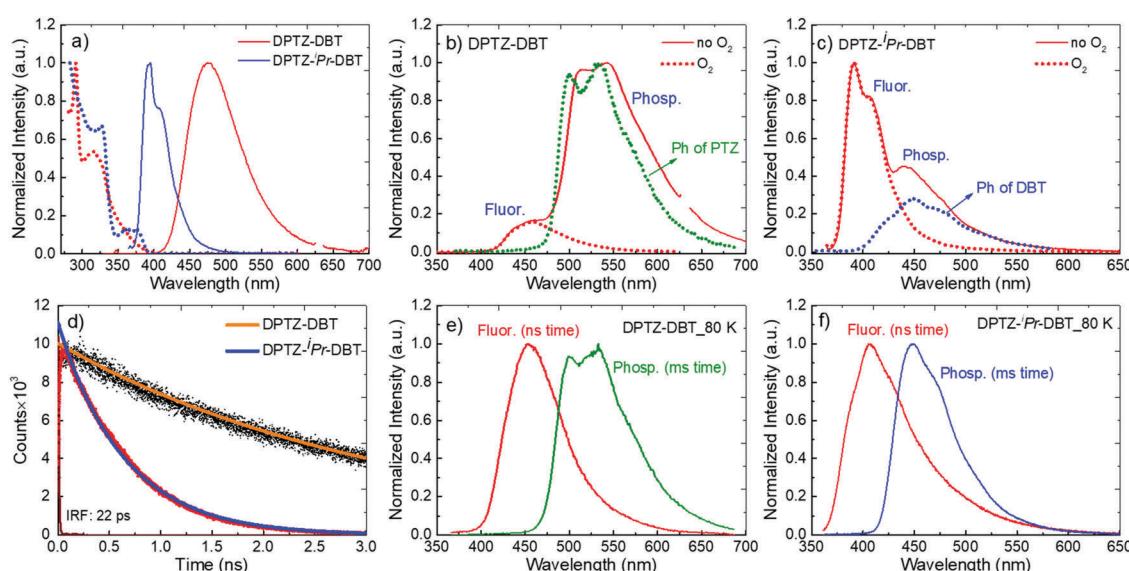

Fig. 3 (a) Absorption and steady-state emission spectra of **DPTZ–DBT** and **DPTZ–ⁱPr–DBT** in toluene at RT. (b) Steady-state emission spectra in zeonex at RT, in air and under vacuum for **DPTZ–DBT**. The phosphorescence of **PTZ** is also shown matching the phosphorescence of **DPTZ–DBT**. (c) Steady-state emission spectra in zeonex at RT, in air and under vacuum for **DPTZ–ⁱPr–DBT**. The phosphorescence of **DBT** unit is also shown matching the phosphorescence of **DPTZ–ⁱPr–DBT**; (d) fluorescence decays of **DPTZ–DBT** and **DPTZ–ⁱPr–DBT**, in toluene solution at RT. (e and f) Time-resolved fluorescence and phosphorescence spectra at 80 K for (e) **DPTZ–DBT**; (f) **DPTZ–ⁱPr–DBT**. The fluorescence and phosphorescence for e and f were collected with delay times of 1.1 ns and 50.1 ms, respectively.

DPTZ–DBT Equatorial Form

DPTZ-ⁱPr–DBT Axial Form
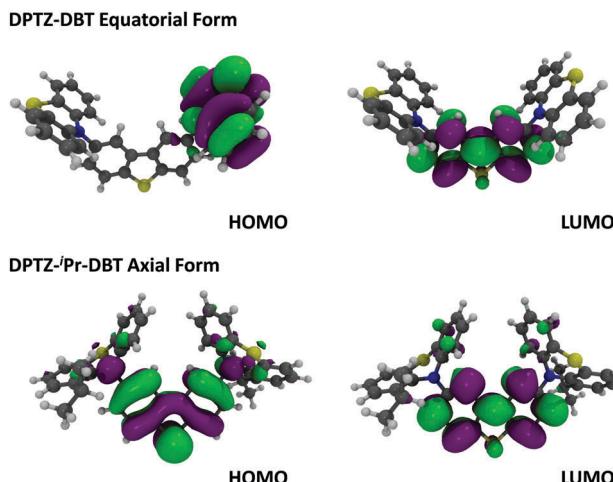
Fig. 4 Molecular orbitals, HOMO and LUMO of **DPTZ–DBT** (equatorial) and **DPTZ–ⁱPr–DBT** (axial) forms at DFT (M062X)/Def2SVP level of theory.

not a charge transfer (CT) transition, as the CT state is clearly not formed in the substituted compounds (see Fig. S3, ESI†). Instead, as shown by the HOMO and LUMO plots in Fig. 4, this transition corresponds mostly to a transition centred on the **DBT** unit, but due to the axial conformation **DBT** mixes with **PTZ**. It is this mixing which explains why the band is absent for the absorption spectra of the two fragments.

Clear and defined differences are observed in the emission spectra in this molecular series. **DPTZ–DBT** shows broad emission in toluene, peaking at 480 nm, which further red-shifts with increasing solvent polarity (Fig. S3a, ESI†). In contrast, the substituted compounds **DPTZ–Me–DBT**, **DPTZ–ⁱPr–DBT** and **DPTZ–^tBu–DBT** show well-resolved, blue-shifted emission, which is entirely independent of solvent polarity (Fig. S3, ESI†). These observations are consistent with the CT character of the lowest singlet excited state in **DPTZ–DBT**, as expected from the HOMO and LUMO orbitals in Fig. 4. In the substituted compounds the excited state has no CT character, based on the absence of solvatochromism in the emission (Fig. S3, ESI†). This observation is also confirmed by the calculations shown in Table S1 (ESI†).

The unsubstituted **DPTZ–DBT** exhibits axial and equatorial forms in the ground state with only a small energy difference between the two conformers (Table S1, ESI†). The axial form shows no shift with the polarity of the solvent in agreement with the calculations shown in Table S1 (ESI†). However, the equatorial form consistently shifts to lower energies with increasing solvent polarity. In **DPTZ–DBT** the lowest singlet excited state, S_1, is equatorial and the calculated emission is 446, 490 and 566 nm in toluene, anisole, and ethanol, respectively. This strong solvatochromism reflects the stronger CT character of the equatorial form (vs. axial) in agreement with the experimental observations (Fig. S3, ESI†). In contrast, the axial conformer has significant local excitonic character on the **DBT** unit at 334 nm, and therefore is unaffected by solvent polarity. The substituted molecules **DPTZ–Me–DBT**, **DPTZ–ⁱPr–DBT** and **DPTZ–^tBu–DBT** in the ground state exist only in the axial form,

which is identified by the absorption at 380 nm. However, they show both axial and equatorial forms in the excited state, although the former is more stable due to the steric hindrance caused by the alkyl groups (Table S1, ESI†).

Fig. 3b shows that the emission of **DPTZ–DBT** is dominated by phosphorescence, peaking around 540 nm. The fluorescence band is also observed, peaking at 450 nm, at a similar energy of the fluorescence of the donor **PTZ**, (Fig. S2a, ESI†). The phosphorescence band in **DPTZ–DBT** matches with the phosphorescence of **PTZ**, showing that the lowest energy triplet state is localized in the **PTZ** unit. In the presence of oxygen, the phosphorescence is quenched and only the fluorescence band at 450 nm is observed.

As for **DPTZ–DBT**, the substituted molecules, **DPTZ–Me–DBT**, **DPTZ–ⁱPr–DBT** and **DPTZ–^tBu–DBT**, show dual-emission in zeonex (Fig. 3c and Fig. S7, ESI†). Fluorescence is clearly observed peaking around 390 nm, and is accompanied by the phosphorescence band, peaking at 450 nm. This contrasts with **DPTZ–DBT** as the phosphorescence in **DPTZ–ⁱPr–DBT** and **DPTZ–^tBu–DBT** matches perfectly with the phosphorescence of the **DBT** unit, and not of **PTZ**. The phosphorescence behaviour in **DPTZ–Me–DBT** is more complex and is discussed in detail below.

The fluorescence lifetime of **DPTZ–DBT** emission in toluene is 10.3 ns, and fluorescence is observed up to 60 ns (Fig. 5a). This is in clear contrast with the fluorescence decay of the substituted molecules **DPTZ–Me–DBT**, **DPTZ–ⁱPr–DBT** and **DPTZ–^tBu–DBT** (Fig. 5), which show fluorescence lifetimes of approximately 600 ps, and where the fluorescence is observed only up to 2.5 ns. The fluorescence decay in the substituted molecules is, therefore, 17 times faster than that of **DPTZ–DBT**.

The fluorescence and phosphorescence bands from **DPTZ–DBT** and **DPTZ–ⁱPr–DBT** in zeonex are observed independently at early and later times, respectively, due to their different lifetimes (Fig. 3e and f). Remarkably, both fluorescence and phosphorescence in **DPTZ–ⁱPr–DBT** are blue-shifted, when compared with the corresponding spectra of **DPTZ–DBT**. However, while the fluorescence does not match entirely the fluorescence of either **DBT** or **PTZ**, the phosphorescence originates from the high energy triplet state that matches the triplet state localized on the **DBT** unit. **DPTZ–Me–DBT** and **DPTZ–^tBu–DBT** show similar emission properties when compared to **DPTZ–ⁱPr–DBT**, and also have a higher triplet energy level, with phosphorescence matching that of the **DBT** unit (Fig. 6, Fig. S4 and S7, ESI†).

The observation of blue-shifted fluorescence and phosphorescence spectra is not the simple effect of substitution on the **PTZ** unit. The absorption, fluorescence and phosphorescence spectra of **PTZ** and 1-alkyl-**PTZ** derivatives are compared in Fig. S5 (ESI†). Only minimal variations in the absorption and emission spectra are observed upon 1-alkyl substitution. Therefore, the substitution of the **PTZ** molecule alone cannot explain the observations made from the molecules in Fig. 1.

Noteworthy, the methyl substituted **DPTZ–Me–DBT** exhibits dual phosphorescence emission properties. The steric effect of the substituent is less pronounced, compared to **DPTZ–ⁱPr–DBT** and **DPTZ–^tBu–DBT** and dual phosphorescence is observed at RT in zeonex film. The steady-state emission spectra of

This journal is © The Royal Society of Chemistry 2018

J. Mater. Chem. C, 2018, **6**, 9238–9247 | 9241
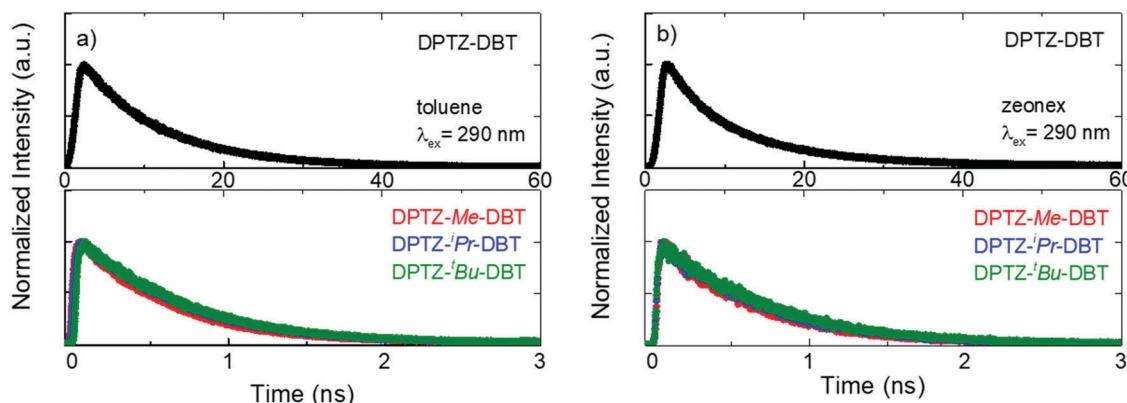
Fig. 5 Emission decays of **DPTZ–DBT**, **DPTZ–Me–DBT**, **DPTZ–ⁱPr–DBT** and **DPTZ–ᵗBu–DBT** collected at the fluorescence bands in air at RT in (a) toluene solution and (b) zeonex film.

DPTZ–Me–DBT (Fig. 6a) show the fluorescence band peaking at 390 nm, as in the case of the other two substituted compounds. However, in **DPTZ–Me–DBT** the fluorescence is accompanied by phosphorescence from the accepting **DBT** unit, peaking at 450 nm, as well as phosphorescence from the donating **PTZ–Me** at 540 nm. The observation of dual phosphorescence is an apparent violation of Kasha's rule.[34]

The fluorescence spectrum of **DPTZ–Me–DBT**, peaks at 390 nm, and was collected at early time (1.1 ns, Fig. 6b). As in the case of **DPTZ–ⁱPr–DBT** and **DPTZ–ᵗBu–DBT**, dual phosphorescence is observed at 50 ms delay-time, composed of low and high energy bands, matching the phosphorescence of **PTZ–Me** and **DBT** respectively (see Fig. 6c). With decreasing temperature, the contribution of **PTZ–Me** phosphorescence

progressively disappears and only the high-energy **DBT** phosphorescence remains at 80 K (Fig. 6c and d).

The phosphorescence behaviour of **DPTZ–Me–DBT** strongly indicates the presence of two conformers in all four **DPTZ–DBT** derivatives, which are separated by a considerable energy barrier. The height of this barrier is very sensitive to the length of the bond between the donor and acceptor groups[18] and therefore while it is high in the ground state, may decrease in the excited state. The axial and equatorial forms are identified in the ground and excited states of **DPTZ–DBT** (see Table S1, ESI†). However, both fluorescence and phosphorescence occur from the most stable state, which is isoenergetic with the **PTZ** singlet and triplet states, and no emission is observed from the high energy state, even at low temperature (Fig. S6, ESI†).
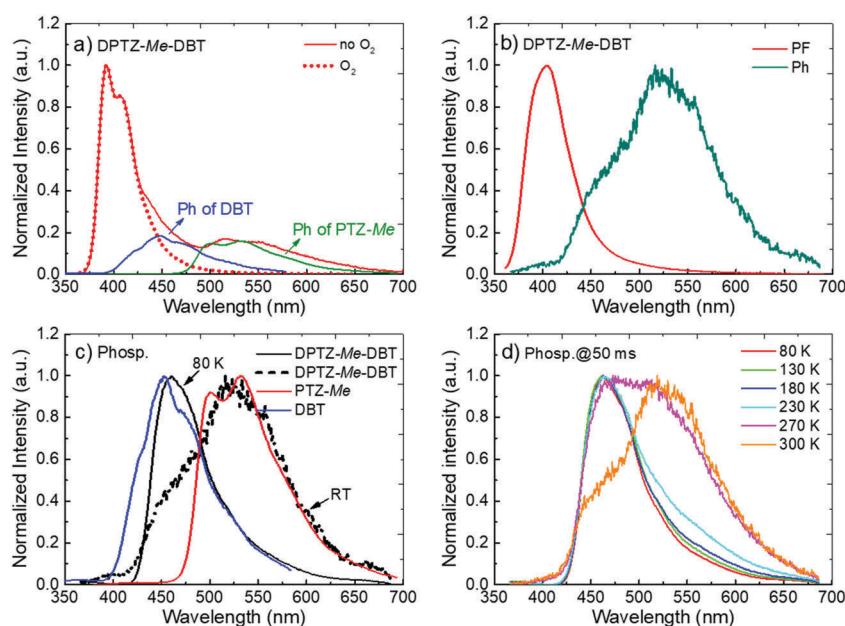
Fig. 6 **DPTZ–Me–DBT** in zeonex film: (a) steady-state emission spectra in air and in vacuum at RT. The phosphorescence of the **DBT** and the **PTZ** units are also shown, matching the two phosphorescence bands in **DPTZ–Me–DBT**. (b) Time-resolved fluorescence and phosphorescence spectra at RT, collected at 1.1 ns and 50 ms, respectively. (c) Phosphorescence spectra at RT and 80 K, compared with the phosphorescence spectra of **DBT** and **PTZ** fragments. (d) Phosphorescence spectra at 50 ms delay-time collected as a function of temperature.

9242 | *J. Mater. Chem. C*, 2018, **6**, 9238–9247

This journal is © The Royal Society of Chemistry 2018

Therefore, the excited state in **DPTZ–DBT** is able to relax to the most stable state, showing no activation barrier. In **DPTZ–Me–DBT** only the axial form is identified in the ground-state. However, both axial and equatorial forms exist in the excited-state (Table S1, ESI†). Interestingly, fluorescence occurs entirely from the higher energy state (when compared with **DPTZ–DBT**). The short lifetime of the singlet excited state does not allow the relaxation to the low energy singlet state to occur. Remarkably, as the triplet state is long-lived, the relaxation to the low energy triplet is possible. Therefore, at high temperatures, **DPTZ–Me–DBT** is able to cross the barrier and gives origin to dual phosphorescence. **DBT**-like phosphorescence is observed peaking at 450 nm, and **PTZ–Me**-like phosphorescence is observed around 530 nm. At low temperatures this relaxation is not possible and consequently only **DBT**-like phosphorescence is observed. This shows that the relaxation between the two triplet states involves an energy barrier separating the two states, which is likely to increase with the bulkiness of the substituents. The fluorescence and phosphorescence from the iso-propyl and tert-butyl substituted compounds, **DPTZ–iPr–DBT** and **DPTZ–tBu–DBT**, confirms this scenario. In these two compounds only the high energy fluorescence and the **DBT**-like phosphorescence are observed, even at RT, as there is insufficient energy available to surmount the barrier. The excited state dynamics in the **DPTZ–DBT** derivatives studied here is summarized in a simplified scheme given in Fig. 7.

Further evidence supporting the switching between the two excited states that are probably associated with the axial and equatorial forms of **DPTZ–DBT** derivatives is obtained from time-resolved phosphorescence decays shown in Fig. 8. In **DPTZ–DBT** the switching involves a vanishingly small energy barrier and the phosphorescence decays mono-exponentially with a 47 ms time constant from the triplet isoenergetic with the **PTZ** phosphorescence (Fig. 8a). However, for the substituted analogues the addition of the alkyl side groups makes switching between the high and low energy excited states sequentially more difficult as the steric hindrance increases. Therefore, the phosphorescence decay of **DPTZ–Me–DBT** shows double exponential profile with a fast component of 6 ms and a long decay component of 37 ms. The fast component progressively disappears with decreasing temperature, with the decay becoming single exponential at low temperature. The phosphorescence decays of **DPTZ–iPr–DBT** and **DPTZ–tBu–DBT** show similar behaviours, although the fast component becomes less important in the most restricted **DPTZ–tBu–DBT**. For the methyl and iso-propyl substituted compounds the dual component of the phosphorescence decays is clearly observed showing a 30% contribution of the fast component with a time constant around 6 ms, and 70% contribution for the long decay component of around 35 ms. The amplitude of the fast component is stronger in the compound carrying the bulkier iso-propyl substituent, relative to the methyl substituted compound. In the more sterically hindered compound substituted with tert-butyl groups the longer decay component contributes above 91% of the phosphorescence decay, and this is practically single exponential decaying with a time constant around 85 ms.

Rates and luminescence yields

Tables 1 and 2, show the photophysical data collected for **DPTZ–DBT**, **DPTZ–Me–DBT**, **DPTZ–iPr–DBT**, and **DPTZ–tBu–DBT** in zeonex solid film and in toluene solution, respectively. The marked decrease on the fluorescence lifetimes (see Fig. 5) are observed due to the pronounced increase on the ISC and IC rates (k_{ISC} and k_{IC}) along the series. In solution, the fluorescence lifetime decreases from 10.3 ns in **DPTZ–DBT** to approximately 600 ps in the substituted **DPTZ–Me–DBT**, **DPTZ–iPr–DBT** and **DPTZ–tBu–DBT**, and in zeonex the behaviour is similar. This is consistent with the increasing oscillator strength of the S_1 state obtained from the calculations, which is 0.0017 for **DPZ–DBT**, and 0.0390, 0.0442 and 0.0451 for **DPTZ–Me–DBT**, **DPTZ–iPr–DBT**
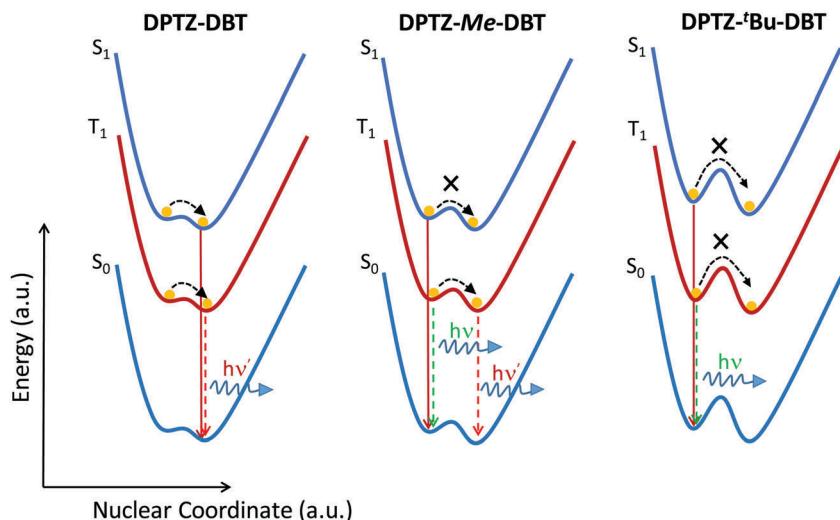

Fig. 7 Schematic representation of the excited state relaxation in the unsubstituted **DPTZ−DBT** and substituted **DPTZ−Me−DBT** and **DPTZ−tBu−DBT**.

This journal is © The Royal Society of Chemistry 2018

J. Mater. Chem. C, 2018, **6**, 9238–9247 | 9243
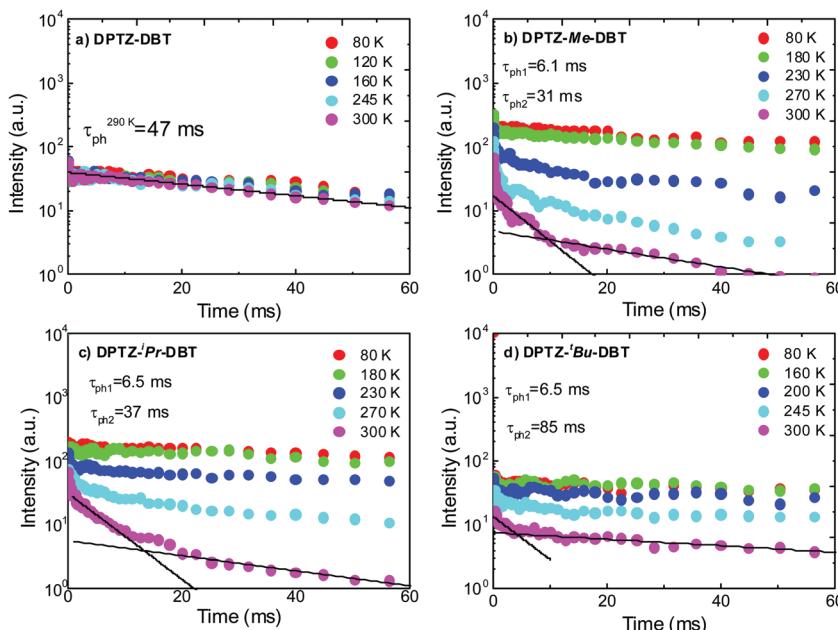
Fig. 8 Time resolved phosphorescence decays in zeonex obtained as a function of temperature for (a) **DPTZ–DBT**, (b) **DPTZ–Me–DBT**, (c) **DPTZ–ⁱPr–DBT** and (d) **DPTZ–ᵗBu–DBT**.

Table 1 Photophysical data of **DPTZ–DBT**, **DPTZ–Me–DBT**, **DPTZ–ⁱPr–DBT**, and **DPTZ–ᵗBu–DBT** in zeonex solid film at RT

Compound	$\Phi_{fl} \pm 0.02$	$\tau_{fl} \pm 0.01$ (ns)	$k_f \pm 0.002$ ($\times 10^9$ s^{-1})	$k_{ISC} \pm 0.01^a$ ($\times 10^9$ s^{-1})	$k_{IC} \pm 0.01$ ($\times 10^9$ s^{-1})	$\Phi_{Ph} \pm 0.08$	Φ_{Lum} (Fluo + Phos)
DPTZ–DBT	0.06	12.60	0.005	0.07	0.004	0.60	0.66
DPTZ–Me–DBT	0.03	0.60	0.050	1.26	0.37	0.01	0.04
DPTZ–ⁱPr–DBT	0.04	0.65	0.061	1.11	0.37	0.02	0.06
DPTZ–ᵗBu–DBT	0.03	0.67	0.045	0.69	0.74	0.02	0.05

^{a} Calculated using Φ_T determined in solution.

Table 2 Photophysical data of **DPTZ–DBT**, **DPTZ–Me–DBT**, **DPTZ–ⁱPr–DBT**, and **DPTZ–ᵗBu–DBT** in toluene solution at RT

Compound	$\Phi_{fl} \pm 0.02$	$\Phi_T^a \pm 0.1$	$\tau_{fl} \pm 0.01$ (ns)	$\tau_T \pm 0.1$ (µs)	$k_f \pm 0.002$ ($\times 10^9$ s^{-1})	$k_{ISC} \pm 0.01$ ($\times 10^9$ s^{-1})	$k_{IC} \pm 0.01$ ($\times 10^9$ s^{-1})
DPTZ–DBT	0.04	0.85	10.29	63.3	0.004	0.08	0.01
DPTZ–Me–DBT	0.03	0.75	0.61	27.6	0.049	1.24	0.36
DPTZ–ⁱPr–DBT	0.02	0.72	0.64	6.2	0.031	1.13	0.41
DPTZ–ᵗBu–DBT	0.02	0.47	0.66	3.5	0.030	0.72	0.77

^{a} Measured in benzene.

and **DPTZ–ᵗBu–DBT**, respectively, and is also indicative of an increase in the locally excited state character of the emitting state. The IC rate (k_{IC}) increases consistently in the series, 1.0×10^7 s^{-1} in **DPTZ–DBT**, 3.7×10^8 s^{-1} in **DPTZ–Me–DBT** and **DPTZ–ⁱPr–DBT**, and 7.4×10^8 s^{-1} in **DPTZ–ᵗBu–DBT**. The radiative rate k_f also increases, but shows no significant variation within the different substituents.

The triplet lifetime in solution also decreases sequentially from 63.3 µs in **DPZ–DBT** to 27.6 µs for **DPTZ–Me–DBT**, 6.2 µs for **DPTZ–ⁱPr–DBT**, and 3.5 µs for **DPTZ–ᵗBu–DBT** (Table 2). This trend is consistent with the enhancement of the IC rate, and the decrease of the phosphorescence efficiency in the substituted molecules, giving indication for the presence of

additional vibrational modes in the substituted molecules, which promote more efficient quenching of the triplet excited state population in **DPTZ–Me–DBT**, **DPTZ–ⁱPr–DBT** and **DPTZ–ᵗBu–DBT**. As a result, the phosphorescence in these compounds is relatively short-lived than in the unsubstituted **DPZ–DBT**, and shows pronounced variation with temperature (Fig. 7).

The total luminescence yield determined in zeonex at RT is much higher in **DPTZ–DBT** ($\approx 66\%$) than in the substituted compounds, for which it is $<6\%$. This is the result of the fast ISC rate and slower IC rate in **DPTZ–DBT**. However, the fluorescence yield is low, even in **DPTZ–DBT** (6%), due to the significantly faster k_{ISC}, when compared to the radiative rate (k_f). In the substituted compounds the ISC rate increases

Table 3 The calculated variable required for eqn (1) and the corresponding k_{ISC}. Due to energy considerations k_{ISC} for **DPTZ–DBT** was calculated in the equatorial and axial forms, while the remaining substituted compounds were calculated in their axial form

Compound	Conformer	SOCME (cm^{-1})	λ (eV)	ΔE_{ST} (eV)	k_{ISC} $(\times 10^9 \ s^{-1})$
DPTZ–DBT	Equatorial	0.10	0.01	0.06	0.014
	Axial	0.80	0.08	0.06	0.015
DPTZ–Me–DBT	Axial	0.80	0.02	0.04	0.209
DPTZ–^{i}Pr–DBT	Axial	1.00	0.01	0.03	0.516
DPTZ–^{t}Bu–DBT	Axial	0.80	0.06	0.02	0.244

significantly and becomes approximately two orders of magnitude faster than the radiative rate, and is surprisingly fast in the methyl substituted **DPTZ–Me–DBT**. The ISC rate in solution, for example, is $8.0 \times 10^7 \ s^{-1}$ for **DPZ–DBT**, $1.24 \times 10^9 \ s^{-1}$ in **DPTZ–Me–DBT**, $1.13 \times 10^9 \ s^{-1}$ in **DPTZ–^{i}Pr–DBT**, and $7.2 \times 10^8 \ s^{-1}$ in **DPTZ–^{t}Bu–DBT**. And in zeonex the behaviour is similar, for **DPTZ–DBT** $k_{ISC} = 7.0 \times 10^7 \ s^{-1}$ and in **DPTZ–Me–DBT** $k_{ISC} = 1.3 \times 10^9 \ s^{-1}$. The rate decreases slightly with increasing bulkiness of the substituent, along with increasing IC rate in the substituted compounds.

To understand the influence of the alkyl substituents on the ISC rates, we have simulated the rate of intersystem crossing using the Fermi golden rule approximation combined with a Marcus formalism to estimate the density of states;

$$k_{ISC} = \frac{2\pi}{\hbar}|\langle\psi_T|\hat{H}_{SO}|\psi_S\rangle|^2 \sqrt{\frac{\pi}{\lambda k_B T}} \exp\left(\frac{(\lambda + \Delta E_{ST})^2}{4\lambda k_B T}\right) \quad (1)$$

Here λ corresponds to the reorganization energy, *i.e.* the energy variation in the initial singlet excited state when switching from the singlet equilibrium geometry to the triplet equilibrium geometry, while the driving force ΔE_{ST} is identified as the adiabatic singlet–triplet gap.[35] The S_1 state is closest in energy to the T_3 state and therefore we consider ISC to occur between these states. The rates to lower triplet states were calculated, but in each case $\Delta E_{ST} > 0.15$ eV yielding very small k_{ISC}.

Using eqn (1) and the calculated data shown in Table 3, we find an ISC rate of $0.014 \times 10^9 \ s^{-1}$ for **DPTZ–DBT**. The rate increases to $0.209 \times 10^9 \ s^{-1}$ for **DPTZ–Me–DBT**, $5.16 \times 10^8 \ s^{-1}$ in **DPTZ–^{i}Pr–DBT**, and $2.44 \times 10^8 \ s^{-1}$ in **DPTZ–^{t}Bu–DBT**. This reveals calculated rates broadly consistent with the experimental observations in that k_{ISC} is larger for the substituted molecules. This is due to the smaller energy gap between the S_1 and T_3 states. While the trends of k_{ISC} for the substituted molecules do not exactly follow experimental observations, these differences are within the uncertainty of the calculations, which due to the exponential dependence of λ and ΔE_{ST} in eqn (1) are very sensitive to small differences in λ and ΔE_{ST}.

The IC rate (k_{IC}) increases consistently in the series, $k_{IC} = 4.0 \times 10^6 \ s^{-1}$, in **DPTZ–DBT**, $k_{IC} = 3.7 \times 10^8 \ s^{-1}$ in **DPTZ–Me–DBT** and **DPTZ–^{i}Pr–DBT**, and $k_{IC} = 7.4 \times 10^8 \ s^{-1}$ in **DPTZ–^{t}Bu–DBT**. Finally, the radiative rate k_f also increases, but shows no significant variation within the different substituents.

Finally, by comparing **DPTZ–DBT** with previously reported carbazole substituted analogue, 3,7-di(*N*-carbazolyl)-dibenzothiophene (**DCz–DBT**),[3] the influence of the sulfur atom in the **PTZ** units is revealed. The presence of **PTZ** induces a pronounced enhancement of the triplet formation yield, and shows no effect on the fluorescence yield. In the case of the **PTZ** H-intra conformation (equatorial form), the nitrogen lone pair is delocalized over the phenyl rings of the **PTZ** unit, which may explain the excellent RTP properties of the **DPTZ–DBT** compound. Marked differences are however observed in the rate constants for radiative decay, k_f, intersystem crossing, k_{ISC}, and non-radiative internal conversion, k_{IC}, all showing a pronounced decrease on **DPTZ–DBT**. The fluorescence decay, for example, decreases from ≈ 10 ns in **DPTZ–DBT** to 0.88 ns in **DCz–DBT**. **DPTZ–DBT** can also be compared with other **PTZ** derivatives using the strong acceptor dibenzothiophene-*S,S*-dioxide (**DBTO2**) unit, where the equatorial form leads to negligible singlet–triplet energy gap and emergence of TADF. However, when the axial form is adopted due to the steric effect of the alkyl groups that block the relaxation of the **PTZ** units in the excited-state, RTP instead of TADF is observed containing contributions from two triplet states matching the phosphorescence of **PTZ** and DBTO2.[32]

Conclusions

In summary, this series of **DPTZ–DBT** luminophores provides new insights into the design of all-organic RTP emitters and demonstrates how systematic changes in the substituents can tune photophysical properties by conformational control. **DPTZ–DBT** and substituted analogues exist in equatorial and axial forms in the ground state. Here, it has been demonstrated that different conformations have markedly different photophysical properties, with the axial conformer showing enhanced ISC rate. This is accompanied by similar acceleration of the radiative and non-radiative IC rates. Switching between electronic excited states occurs with a vanishingly small barrier in the unsubstituted **DPTZ–DBT**. However, an increasing barrier is imposed by the presence of the bulkier side groups, and this mainly prevents the relaxation of the singlet and triplet excited states to lower energy in these substituted compounds.

The unsubstituted molecule **DPTZ–DBT** shows dual emission, fluorescence and strong green phosphorescence, in solid zeonex film at RT, with a high total luminescence yield of $\approx 66\%$. The triplet formation yield is the highest in the series (85%), and the fluorescence and phosphorescence lifetimes are relatively long-lived, 12.6 ns and 47 ms, respectively, resulting in relatively slow excited state decay rates, but dominant ISC. This behavior is markedly altered by tuning of the conformation due to the presence of bulky side groups in the C(1)-position of each **PTZ** unit. The substituted molecules show much shorter fluorescence and phosphorescence lifetimes due to faster radiative, IC and ISC rates, and also low luminescence yields, and notably, higher singlet and triplet energies. Interestingly, the molecule substituted with the less bulky

This journal is © The Royal Society of Chemistry 2018

J. Mater. Chem. C, 2018, **6**, 9238–9247 | 9245

methyl group, **DPTZ–Me–DBT**, in addition to fluorescence, shows also dual phosphorescence at RT. This originates from T_1 in the green region, at 2.60 eV, coincident with the emissive triplet of **DPTZ–DBT**, and from T_2 in the blue region, at 2.88 eV, approximately the same energy of the emissive triplet in **DPTZ–^{i}Pr–DBT** and **DPTZ–^{t}Bu–DBT**. This is an apparent violation of Kasha's rule imposed by the existence of different conformers. However, at low temperatures, only the high energy blue phosphorescence is observed as there is insufficient energy to drive the relaxation of the excited state. In conclusion, the strategy of selective functionalization of the donor unit is shown to be a viable approach to tuning the excited state properties of D–A molecules for RTP emission, including blue emitters.

Author contributions

R. H. performed the majority of the optical measurements under the supervision of F. B. D. J. W. and N. A. K. synthesized molecules under the guidance of M. R. B. and carried out NMR studies. J. A., J. C. L. and M. N. B.-S. carried out Flash-Photolysis studies and determined triplet formation and luminescence quantum yields. A. S. B. performed the X-ray characterization. The full physical model was devised by J. W., T. J. P. and F. B. D., and it was theoretically tested within a quantum chemistry framework by J. G. and T. J. P. F. B. D. wrote the manuscript, which was revised by all the co-authors.

Conflicts of interest

There are no conflicts of interest to declare.

Acknowledgements

References

1 R. Kabe, N. Notsuka, K. Yoshida and C. Adachi, *Adv. Mater.*, 2016, **28**, 655–660.

2 S. Hirata and M. Vacha, *Adv. Opt. Mater.*, 2017, **5**, 1600996.

3 R. Huang, J. Avó, T. Northey, E. Chaning-Pearce, P. L. dos Santos, J. S. Ward, P. Data, M. K. Etherington, M. A. Fox, T. J. Penfold, M. N. Berberan-Santos, J. C. Lima, M. R. Bryce and F. B. Dias, *J. Mater. Chem. C*, 2017, **5**, 6269–6280.

4 B. Xu, H. Wu, J. Chen, Z. Yang, Z. Yang, Y.-C. Wu, Y. Zhang, C. Jin, P.-Y. Lu, Z. Chi, S. Liu, J. Xu and M. Aldred, *Chem. Sci.*, 2017, **8**, 1909–1914.

5 Z. Yang, Z. Mao, X. Zhang, D. Ou, Y. Mu, Y. Zhang, C. Zhao, S. Liu, Z. Chi, J. Xu, Y. C. Wu, P. Y. Lu, A. Lien and M. R. Bryce, *Angew. Chem., Int. Ed.*, 2016, **55**, 2181–2185.

6 G. Zhang, G. M. Palmer, M. W. Dewhirst and C. L. Fraser, *Nat. Mater.*, 2009, **8**, 747–751.

7 O. S. Wolfbeis, *Adv. Mater.*, 2008, **20**, 3759–3763.

8 Y. Feng, J. Cheng, L. Zhou, X. Zhou and H. Xiang, *Analyst*, 2012, **137**, 4885.

9 L. Jethi, M. M. Krause and P. Kambhampati, *J. Phys. Chem. Lett.*, 2015, **6**, 718–721.

10 K. Okabe, N. Inada, C. Gota, Y. Harada, T. Funatsu and S. Uchiyama, *Nat. Commun.*, 2012, **3**, 705–709.

11 S. Reineke, N. Seidler, S. R. Yost, F. Prins, W. A. Tisdale and M. A. Baldo, *Appl. Phys. Lett.*, 2013, **103**, 93302.

12 S. R. Forrest, M. A. Baldo, D. F. O'Brien, Y. You, A. Shoustikov, S. Sibley and M. E. Thompson, *Nature*, 1998, **395**, 151–154.

13 Y. Liu, G. Zhan, P. Fang, Z. Liu, Z. Bian and C. Huang, *J. Mater. Chem. C*, 2017, **5**, 12547–12552.

14 S. Mukherjee and P. Thilagar, *Chem. Commun.*, 2015, **51**, 10988–11003.

15 W. Zhao, Z. He, J. W. Y. Lam, Q. Peng, H. Ma, Z. Shuai, G. Bai, J. Hao and B. Z. Tang, *Chem*, 2016, **1**, 592–602.

16 H. Uoyama, K. Goushi, K. Shizu, H. Nomura and C. Adachi, *Nature*, 2012, **492**, 234–238.

17 F. B. Dias, T. J. Penfold and A. P. Monkman, *Methods Appl. Fluoresc.*, 2017, **5**, 12001.

18 T. J. Penfold, F. Dias and A. P. Monkman, *Chem. Commun.*, 2018, **54**, 3926–3935.

19 A. S. D. Sandanayaka, T. Matsushima and C. Adachi, *J. Phys. Chem. C*, 2015, **119**, 23845–23851.

20 A. S. D. Sandanayaka, K. Yoshida, T. Matsushima and C. Adachi, *J. Phys. Chem. C*, 2015, **119**, 7631–7636.

21 A. Stockmann, J. Kurzawa, N. Fritz, N. Acar, S. Schneider, J. Daub, R. Engl and T. Clark, *J. Phys. Chem. A*, 2002, **106**, 7958–7970.

22 M. K. Etherington, F. Franchello, J. Gibson, T. Northey, J. Santos, J. S. Ward, H. F. Higginbotham, P. Data, A. Kurowska, P. L. Dos Santos, D. R. Graves, A. S. Batsanov, F. B. Dias, M. R. Bryce, T. J. Penfold and A. P. Monkman, *Nat. Commun.*, 2017, **8**, 14987.

23 H. Tanaka, K. Shizu, H. Nakanotani and C. Adachi, *J. Phys. Chem. C*, 2014, **118**, 15985–15994.

24 S. Gan, W. Luo, B. He, L. Chen, H. Nie, R. Hu, A. Qin, Z. Zhao and B. Z. Tang, *J. Mater. Chem. C*, 2016, **4**, 3705–3708.

25 M. Okazaki, Y. Takeda, P. Data, P. Pander, H. Higginbotham, A. P. Monkman and S. Minakata, *Chem. Sci.*, 2017, **8**, 2677–2686.

26 F. B. Dias, J. Santos, D. R. Graves, P. Data, R. S. Nobuyasu, M. A. Fox, A. S. Batsanov, T. Palmeira, M. N. Berberan-Santos, M. R. Bryce and A. P. Monkman, *Adv. Sci.*, 2016, **3**, 1600080.

27 F. B. Dias, S. King, A. P. Monkman, I. I. Perepichka, M. A. Kryuchkov, I. F. Perepichka and M. R. Bryce, *J. Phys. Chem. B*, 2008, **112**, 6557–6566.

28 L. Wang, Z. Y. Wu, W. Y. Wong, K. W. Cheah, H. Huang and C. H. Chen, *Org. Electron.*, 2011, **12**, 595–601.

9246 | *J. Mater. Chem. C*, 2018, **6**, 9238–9247

This journal is © The Royal Society of Chemistry 2018

29 H. W. Lee, S. Jeong, S. E. Lee, Y. K. Kim and S. S. Yoon, *Jpn. J. Appl. Phys.*, 2016, **55**, 06GK07.

30 J. Guo, X.-L. Li, H. Nie, W. Luo, S. Gan, S. Hu, R. Hu, A. Qin, Z. Zhao, S.-J. Su and B. Z. Tang, *Adv. Funct. Mater.*, 2017, **27**, 1606458.

31 F. B. Dias, K. N. Bourdakos, V. Jankus, K. C. Moss, K. T. Kamtekar, V. Bhalla, J. Santos, M. R. Bryce and A. P. Monkman, *Adv. Mater.*, 2013, **25**, 3707–3714.

32 J. S. Ward, R. S. Nobuyasu, A. S. Batsanov, P. Data, A. P. Monkman, F. B. Dias and M. R. Bryce, *Chem. Commun.*, 2016, **52**, 2612–2615.

33 X. Tang, T. Shan, Q. Bai, H. Ma, X. He and P. P. Lu, *Chem. – Asian J.*, 2017, **12**, 552–560.

34 M. Kasha, *Discuss. Faraday Soc.*, 1950, **9**, 14–19.

35 D. Beljonne, Z. Shuai, G. Pourtois and J. L. Bredas, *J. Phys. Chem. A*, 2001, **105**, 3899–3907.